Proceedings of the ASME 2010 3rd Joint US-European Fluids Engineering Summer Meeting and 8th International Conference on Nanochannels, Microchannels, and Minichannels
FEDSM-ICNMM2010
August 1-5, 2010, Montreal, Canada

FEDSM-ICNMM2010-30512

INVESTIGATION OF EFFECTS OF RADIAL DISTORTION ON TRANSONIC FAN BEHAVIOR

Dmytro M. Voytovych
Purdue University
West Lafayette, Indiana, USA

Guoping Xia
Purdue University
West Lafayette, Indiana, USA

Chenzhou Lian
Purdue University
West Lafayette, Indiana, USA

Charles L. Merkle
Purdue University
West Lafayette, Indiana, USA

ABSTRACT

The flow analysis around blades of a transonic fan is presented for both clean and radially distorted inlets. Computations are shown for four-blade passages that are accomplished with a second order accurate code using a k-ω turbulence model. The mass flow rate along a speed line is controlled by varying a choked nozzle downstream of the fan. The results show good agreement with data for three speed lines. In the near-stall region, the flow first becomes unsteady and then unstable with the unsteadiness increasing at lower speeds. The four-blade simulations remained stable to lower mass flow rates than the single-blade simulations. In the near-stall vicinity, tip vortex breakdown occurred creating a low momentum zone near the blade tip on the pressure side that grew as the mass flow was decreased until it eventually blocked the passage. The presence of distortion reduced the operational range and moved the stall line to higher mass flow rates. At high speeds distortion reduced both the mass flow rate and total pressure ratio while at lower speeds, the choking mass flow rate was reduced, but the total pressure ratio was slightly improved. The flow separation near the hub on the suction side was caused by the distortion. Its size was decreasing with rotational speed.

INTRODUCTION

The development of a new low boom supersonic aircraft requires that existing jet engines be used in conjunction with a supersonic inlet that decelerates the flow from supersonic to subsonic conditions [1]. The shock from the inlet lip and the boundary layers on the much longer center body produces significantly stronger flow non-uniformities in the supersonic case than for a subsonic inlet. The performance and stability range of the engine change under these conditions and is of great concern to designers. In particular, questions of interest are how the fan, which is affected first, responds and transmits these distortions. Thus, detailed understanding of the flow around the fan is necessary to provide information for developing control techniques that ensure desirable performance and operation.

The effects of inlet distortion have been addressed by numerous previous authors ([6]-[10]) most of which have been experimental in nature. In general it was found that the severity of degradation of the total pressure ratio and operating range depends on type of the distortion and that the response of different compressors to the same distortion depended on the type of stall inception they exhibit. Only a few experiments were performed on high transonic compressors for example as described by Hah *et al.* [8].

In addition to experimental studies a limited number of computational studies have also looked at the effects of distortion on performance and stall inception ([3], [9]-[11]). In general, the inlet distortions vary both circumferentially and radially requiring full wheel unsteady simulations. This demands significant computational resources and increases pre/post-processing of the occurred data. As an initial step for more general simulations, we focus first on radial distortion effects.

In the present work an isolated fan blade row is studied using four blade passages with reference simulations for a single blade passage included for completeness (for single

blade results see Ref. [12]). To address the effects of shock strength three speed lines at high rotational speeds were computed from choke to stall with both clean and radial distortion profiles. In previous investigations artificial distortion profiles were generally considered. In the present work, the profiles were obtained from rig test results that used screens to simulate both tip and hub deficits of total pressure. The focus is on evaluating the effects of radial distortion on performance and stall margin along three speed lines to provide insight into the flow structure. For validation, the predicted performance is compared with available experimental data.

COMPUTATIONAL METHOD

An in-house code [13] that solves the compressible unsteady Reynolds-Averaged Navier-Stokes equations was used for the simulations. The equations were written in terms of the absolute velocity components in the relative frame rotating at a constant angular velocity similar to Chen *et al.* [15]. The governing equations are discretized in space by a finite volume method on an unstructured grid with an approximate Riemann solver used for reconstructing the fluxes at the faces of each control volume. Temporal discretization was accomplished by means of a three-point backward stencil ([13] and [14]). An implicit dual-time method was used to eliminate factorization errors in unsteady calculations. The effects of turbulence were incorporated by means of the $k-\omega$ model [16].

The computational domain is determined by the hub, casing, periodic surfaces and the inlet and outlet boundaries. An important issue, especially for high transonic conditions that generate strong shocks that propagate considerable distances upstream of the stage, is to ensure that disturbances do not reflect from the upstream and downstream boundaries. In the present calculations, reflections were precluded by placing the boundaries far upstream and downstream of the blade row and using strong grid stretching to ensure outgoing waves damped before reaching the boundary.

Because the traditional radial equilibrium condition at the outlet boundary is not applicable in unsteady flow, the downstream portion of the flow channel was extended in a manner similar to [11] and a choked nozzle followed by a short diverging length was placed at the outlet boundary as proposed by Vahdati *et al.* [17]. This avoids the uncertainty of radial equilibrium and allows natural development of the flow downstream of the blade row for both steady and unsteady flow. A meridional view of the computational domain is shown in Fig. 1a.

The domain was discretized using an unstructured grid with hexahedral cells. The topology of the grid at each streamwise location is similar to an H-O-H type grid as shown in Fig. 1b. The dimensions were 193 nodes around the blade, 65 nodes in the blade to blade direction and 104 nodes in the span direction. The tip clearance was filled with several H-blocks with 17 nodes in the spanwise direction in the tip clearance. This allows efficient meshing of complex blade shapes, adequate resolution of viscous boundary layers and is suitable for partitioning during parallel computations. A total 6,000,000 nodes was used for the four blade calculations. The shape of the converging/diverging part of the exit nozzle was adjusted from inside the code to move along or between speed lines without need for re-gridding. This arrangement was useful when approaching the stall margin. The total pressure, total temperature and flow angles were prescribed at the inlet boundary. Periodic boundaries were treated without time delay. The blade geometry was taken as representative of a modern high bypass ratio fan configuration and a fixed blade shape was used for all speed lines.

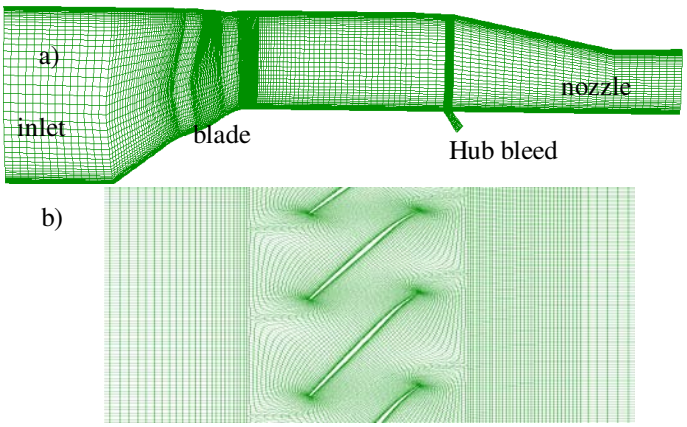

Figure 1. Computational grid: a) meridian view with choked nozzle and hub bleed channel; b) H-O-H grid.

The computations were started from the choke condition using the steady solver and solutions were run sequentially along a given speed line toward stall. Convergence was monitored closely as the blade loading increased, and at the point on the speed line where convergence started to deteriorate, the solver was switched from steady to unsteady. The single blade simulations helped to identify points on the map where this could be expected to happen for the four blade calculations. Steady computations were converged for five orders of magnitude. Time-accurate computations were continued for at least 10 full wheel revolutions with a resolution of 700 steps per revolution. The criteria for stall/unstable flow conditions in computations was a drop in mass flow rate of more than 5% from the last point on the map and the development of substantial flow separation near the blade tip.

During unsteady computations the mass flow rate and the mass averaged static and total pressure and temperature were monitored at axial positions one blade chord upstream and downstream of the blade and at the inlet and outlet boundaries.

In addition, several local "probes" were placed in the vicinity of the blade tip and at mid span to monitor unsteady behavior.

RESULTS AND DISCUSSION

Three speed lines, 100, 95 and 80%, were analyzed. Representative results for each line are presented for both clean and radially distorted inflows. The results from the three speed lines are then compared to identify similarities and differences. The total pressure ratio and corrected mass flow rates on all performance maps shown below have been non-dimensionalized by design point conditions.

The four blade simulations artificially limit the longest circumferential wave to part of the circumference so that modal stall inception cannot be computed correctly, however, as shown by several authors ([19]-[17]) valuable information up to stall inception can be obtained and even spike stall can be analyzed with a single or several blades.

Distortion profiles

Four characteristic inlet distortion profiles for the present geometry are shown in Fig. 2. These include a 'clean' inlet with small losses representative of those incurred in a subsonic inlet, two profiles taken from experiments with screens designed to simulate the effects of a supersonic inlet, and one profile taken from a computational analysis of a supersonic inlet [2] that is included for reference. The losses induced by the screen were quite strongly dependent on the mass flow rate and were higher at choke and lower near stall as can be seen in Fig. 2. At choke conditions, the maximum total pressure losses were 15% near the hub and 10% near the tip respectively with a radial extension of approximately 30% from hub and tip. The average total pressure was about 4% lower than the clean value. At near-stall conditions the maximum losses were 5% near the hub and 3% at the tip with a radial extension around 20%. The computational profile corresponds to the design condition and is in reasonable agreement with the near-choke screen distribution. The present calculations are based upon two of these profiles with one exception. The 'clean' inlet profile was used for all 'clean' inlet calculations, while the near-choke distortion was used along the entire speed line for the distorted inlet calculations. In addition, one example solution with the near-choke distortion profile is given at 100% speed to identify the effects of the varying distortion on computed performance.

100% Speed

We start with conditions on the 100% speed line which corresponds to a relative rotor tip Mach number of 1.4. The characteristic lines are shown in Fig. 3 and include both experimental data and computational predictions for clean and distorted inlet. In addition, computational results are shown for both single- and four-blade computations.

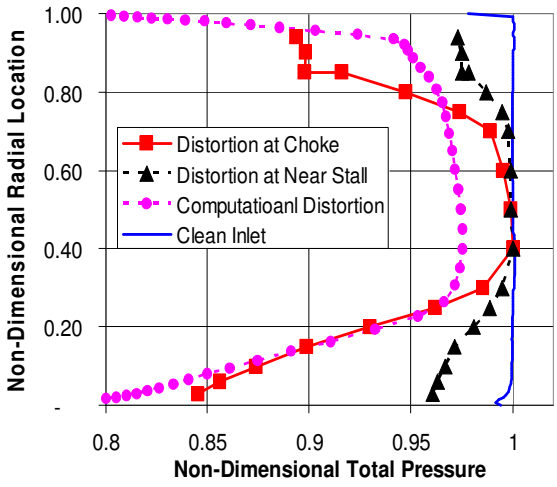

Figure 2. Total pressure profiles for clean and distorted inlets.

The clean results agree well with experiment through the whole range of the mass flow rate for this speed. In the experiments, surge occurred between the last indicated point on the characteristic and the stall/surge margin. The single blade computations went approximately half-way between the last experimental point and the stall line, while the four-blade simulations allowed steady solutions all the way to the stall margin. The slope of the characteristic remained negative in the single blade case while it changed from negative to positive when approaching margin in the four-blade simulations. The change in slop suggest that the fan might exhibit modal stall, but the flow break down occurred without developing rotating pattern nearly simultaneously in all four passages similar to findings in Ref. [21]. The difference was that in this case we did not observe any unsteady flow oscillations prior to stall/surge onset. The way how the transition occurred is can be explained by the presence of strong front shocks that do not allow communication between the passages from the upstream and thus no flow redistribution occurs. The Mach number contours and velocity distribution near the tip are given later to demonstrate this.

A comparison of solutions with two different radial distortions, one with the near-choke distribution from Fig. 2 and one with the near-stall distribution, is also included in Fig. 3 for the single-blade calculations. As noted above, these represent the largest and smallest distortions from the experiment and, as can be seen, these two limits of the distortion bracket the experimental data. At near-choke conditions the computations with the near-choke profile are quite close to the experiment, indicating the computations are predicting the impact of the distortion accurately. At the near-stall condition the results with the near-stall profile are again similar to experiment, although the effect of the distortion is quite small. In terms of the effect of distortion on the operating

point, the simulation slightly over predicts the total pressure ratio and flow rate by approximately 1%.

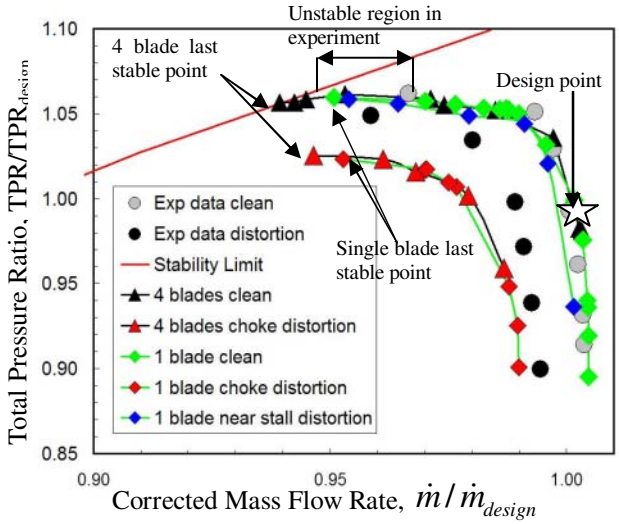

Figure 3. Performance map of 100% speed line.

The effect of the distortion in the four blade simulations was similar to the single blade along the speed line with a small difference near the stability limit. The four passage calculations resulted in a flow rate at the last stable point that was approximately 1% lower than that obtained with the single blade calculation.

The total pressure ratio distribution along the span at the exit is shown in Fig. 4 for four blades at the design point and at near-stall conditions. For the clean inlet, the pressure ratio near the hub is almost constant and the work by blade is produced mainly by the upper part of the blade as the load increases. The effect of the total pressure deficit from the distortion at the design point appears near the hub and at the upper part of the blade span from tip to the midspan. Near the hub a 15% total pressure deficit produced 25% total pressure ratio drop. This is mainly because of the hub stall on the suction side. At the upper part of the span distortion decreased the total pressure ratio by 5%. The initial total pressure deficit at 25% span grew to almost 50% at the fan exit. At near-stall, the pressure deficit near the hub extends slightly upwards, but the maximum deficit remained almost the same. At the upper part of the span, the pressure decreased almost uniformly by approximately 4%.

Figure 5 shows contours of the Mach number near the tip together with constant Mach number 0.2 surface and stream lines. The flow structure around the fan blades is similar to other transonic blades (see for example Chima [24], Adamczyk *et al* [25]) and we just emphasize the near tip region, where a low momentum zone develops near the pressure side at low flow rates where it contributes to passage blockage [23]. The difference from the compressor blade in Ref. [23] was that the leading edge vortex broke down inside the low momentum zone and not just overflowing it. Contours of the Mach number at 99% blade span are shown in Fig. 6 at near stall conditions with a clean inlet. The low momentum zone occupied more than 50% of the passage. This is considerably much more the separated flow on the suction side.

To see how this low momentum zone develops and the effect of distortion on it, the circumferential distribution of axial velocity is shown in Fig. 7 along 20% chord taken at the 99% span location. The four lines shown in the figure represent conditions at the design point and near stall for the clean inlet and for the solution with distortion. Considering the clean inlet results first, we see that the suction side the velocity reaches a maximum, then decreases approaching the pressure side. The velocity exhibits a spike at a location 25% of the pitch away from the pressure side as the flow traverses the bow shock. At near stall conditions, the velocity near the suction side increases slightly, but on the pressure side of the passage the flow reverses and the velocity is negative. This second part corresponds to the region where the tip vortex from the leading edge passes through the bow shock leading to vortex break down.

Radial distortion has a stronger effect on velocity near the design point where it causes a decrease in the velocity near the pressure side. However, the velocity near the suction side remains nearly unchanged. At lower flow rates, the velocity profiles look very similar for the clean and distorted inlets.

Figure 8 represents the instantaneous Mach number contours near the hub taken along the stream surface to illustrate the development of the hub corner stall. This massive flow separation was induced by distortion and caused the observed deficit of the total pressure near the hub in Fig. 4. Contrary to Ref. [8] this separated flow did not propagate along the suction side toward the tip. The span-wise extent of this separation zone was around 10-15% from the hub. Also, the difference between the blades is noticeable. Another separation region develops near the hub leading edge. This separation was also present in the clean results and is caused by the increased incidence of the flow at the lower flow rate.

95% Speed

This speed line represents conditions of the blade with somewhat lower loading and a tip Mach number of 1.33. The flow structures were similar to those at full speed, so only a few noticeable differences are discussed. The performance map for clean and distorted inlets at 95% speed is shown in Fig. 9 for both four-blade and single-blade computations together with the available experimental data in a format analogous to that for the 100% speed line in Fig. 3. As before, the clean results for the four- and single-blade solutions are consistent through the whole operating range from choke to stall. The clean results agree very well with the experimental data and are also very close to the experimental stall margin. It should

be pointed that, unlike conditions at 100% speed, the solutions at the last two points for both single- and four blade calculations were unsteady and were computed using the unsteady solver. The source of the unsteadiness was in the near-tip region and arose because of small oscillations of the tip vortex. Near the hub the flow remained steady.

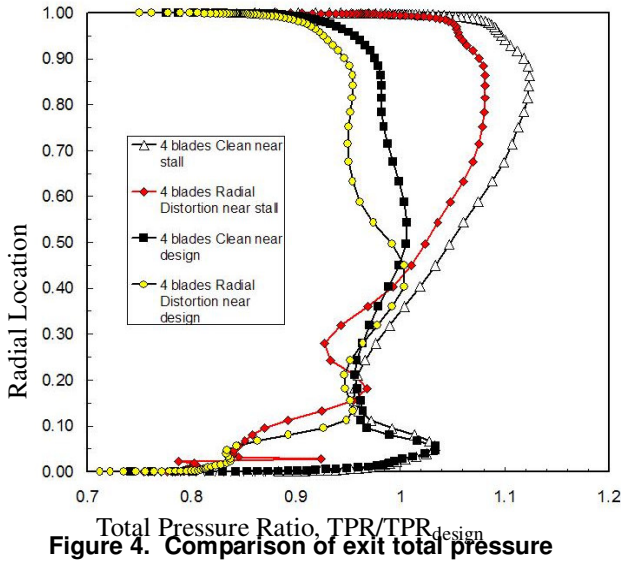

Figure 4. Comparison of exit total pressure ratio, 100% speed.

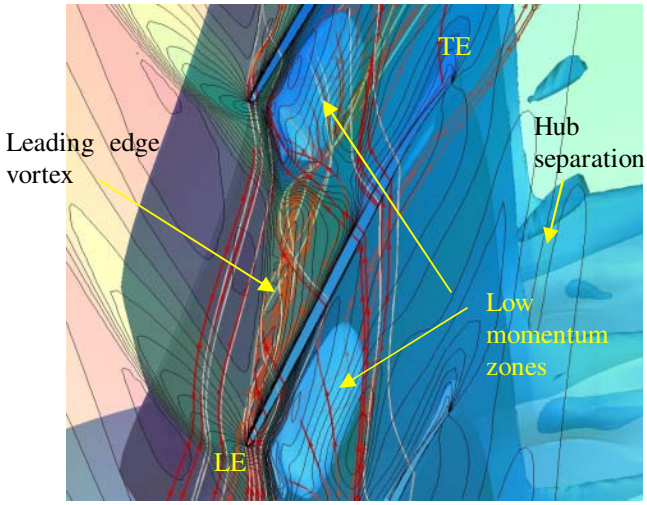

Figure 5. Mach number contours near stall at 99% span with distortion and constant Mach number 0.2 surface, 100% speed.; 99% of blade span.

Applying the distortion had a similar effect on reducing the choke flow mass flow and total pressure ratio and making the flow more unsteady at lower flow rates. The difference is that the shape of the characteristic changes slope from negative to positive going from high to lower flow rates. The location and value of the maximum total pressure rise was different between the single- and four-blade solutions because the flow in the four blade calculation was redistributed between the blades. This redistribution can be seen in Fig. 10 which shows the instantaneous relative Mach number contours at the 99% span location for the last stable (but unsteady) point. Note that the size of the low momentum zone in the passage between the first and second blades on the left is significantly larger than in other passages. The axial velocity at the center of this zone has a much higher negative value.

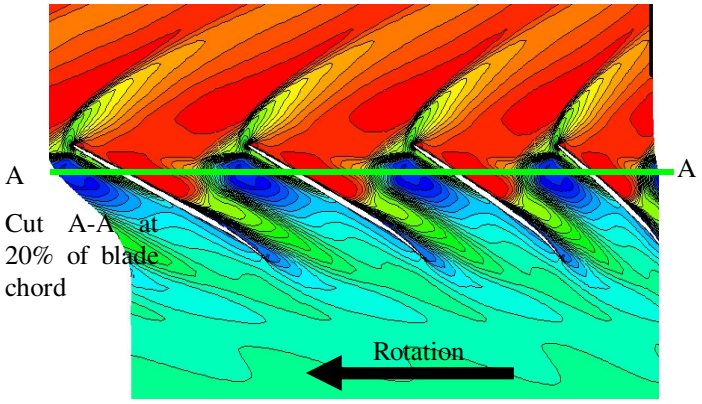

Figure 6. Mach number contours near stall at 99% span with clean inlet, 100% speed.; 99% of blade span.

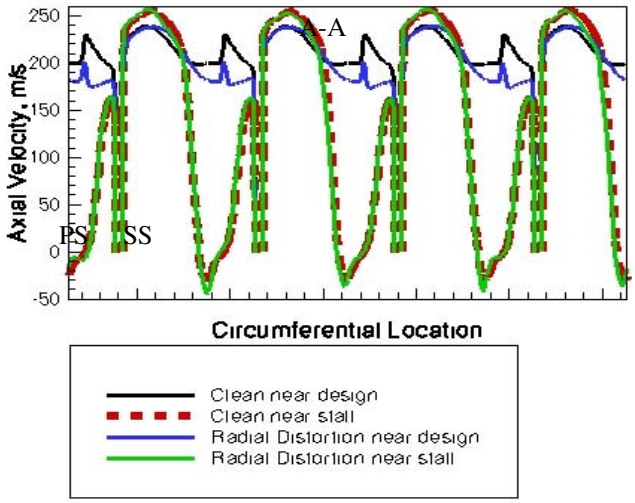

Figure 7. Axial velocity distribution along 20% chord cut at 99% span, 100% speed.

Another similarity to the 100% speed line results was that the distortion again produced a hub corner stall on the suction side. The size of this separation region was smaller than at the 100% speed line with a reduced amount of unsteadiness contrary to the increased level of unsteadiness near the tip.

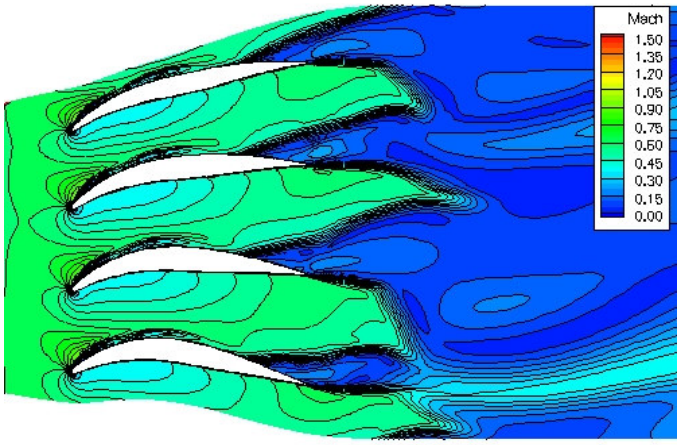

Figure 8. Instantaneous Mach number distribution near the hub with radial distortion near stall, 100% speed.

80% Speed

For the 80% speed line the rotor tip Mach number was 1.12. The performance map is shown in Fig. 11 for a clean inlet and with distortion for four blades and a single blade. The results are again compared with experimental data which is available only for the clean inlet.

The four- and single-blade solutions for the clean inlet are consistent from high to low flow rates where steady solutions were obtained, but show a slight difference near stall where unsteadiness was encountered. Several unsteady solutions with flow oscillations were obtained as shown in the region in Fig. 11 marked as the 'unsteady region.' For the four-blade calculations, the last stable point occurred at a slightly higher flow rate than for the single blade, but it was also unsteady with flow oscillations similar to the single blade results. For these near-stall points, the unsteady performance parameters have been time averaged.

The computations over-predict the total pressure ratio near choke, but are in good agreement with experiment at lower flow rates conditions. The discrepancy is probably due to not accounting the untwist of the blade geometry from full speed conditions.

Figure 11 shows that the presence of radial distortion had a somewhat different effect at the two ends of the speed line. At the near-choke limit, radial distortion caused both the pressure ratio and the mass flow to decrease and the solutions were steady. At the lower flow rates, the total pressure ratio increased slightly over that for the clean inlet. Similar results were observed for other fan in Ref. [5], but here the range of flow rate was larger. In addition, several solutions at lower flow rates became unsteady similar to the clean results, however, the flow went into stall substantially sooner than for the clean inlet computations. The location of the last stable point in the case with radial distortion was at a lower flow rate for four blades than for the single blade solution, analogous to observations at other speeds. However, the slope of the characteristic remains constant at this speed line.

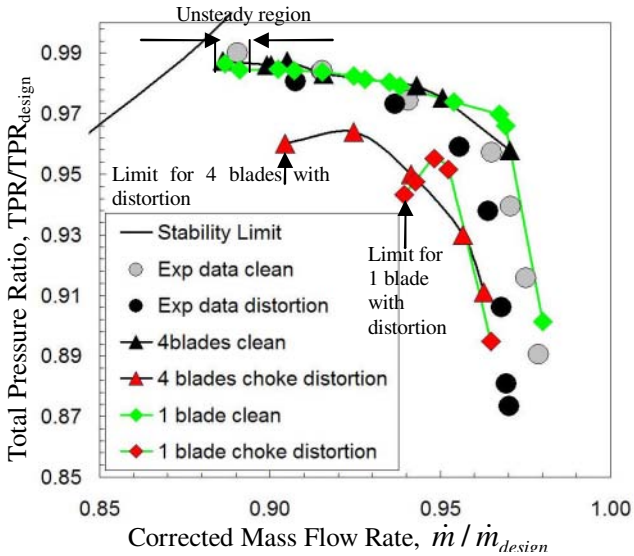

Figure 9. Performance map for 95% speed.

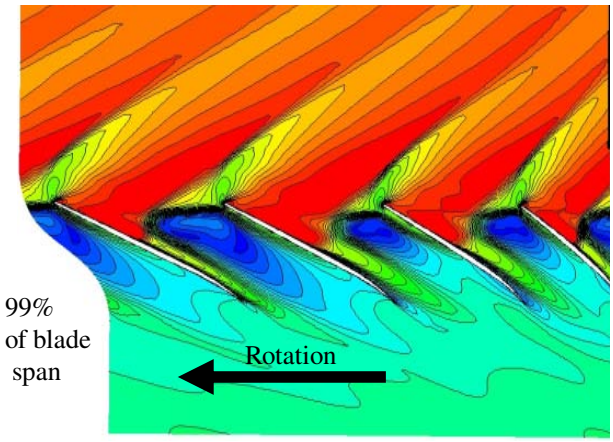

Figure 10. Mach number contours near stall at the 99% span locations at 95% speed with radial distortion inlet.

Next, the total pressure distribution at the exit of the fan is shown in Fig. 12. Near the hub the total pressure remained almost constant at high and near stall flow rates for clean inlet conditions. The blade loading increased above the 15% span

going from high to low flow rate similar to the full speed results.

The effect of the distortion near the hub was different than at the previous two speeds. The flow remained clean after applying the distortion and the peak total pressure decreased by only 3% at high flow rate. At near-stall conditions, the difference between clean and radial distortion was even less.

The effect of the distortion on the portion of the blade above 15% span was qualitatively similar to the 100% speed results at high flow rate. The total pressure increased slightly between 15 and 45% span but decreased between 65 and 90%. At near stall conditions, the effect of distortion is different from the full speed results. The total pressure decreased noticeably only above 65% of the span whereas at the full speed condition it decreased almost uniformly over the upper 80% of the span.

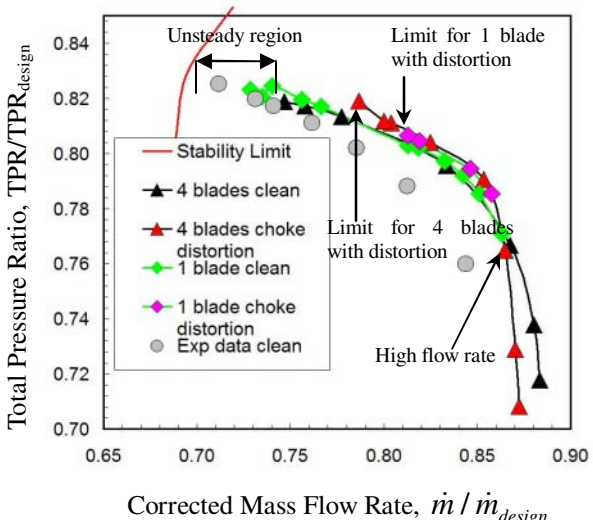

Figure 11. Performance map for 80% speed.

The effect of the near tip deficit is stronger at lower flow rate near stall increasing the effect of interaction of the bow shock and the tip leading edge vortex. This can be seen in Fig. 13 where results at near stall are compared for clean (top) and radial distortion (bottom) solutions. As the flow rate is reduced, the shock moves upstream and the tip vortex also moved upstream to tip leading edge plane. The level of Mach number inside the low momentum zone in passages between the first and second left blades (passage 1), and between the forth blade and through the periodic boundary (passage 4) for the clean results is higher than for the distorted case.

A cut through the 20% chord location taken at 99% span and is shown in Fig. 14. Figure 14 illustrates the axial flow distribution for clean and distorted inlets at high and low flow rates. Going from the suction side to the pressure side the velocity reduces due to the bow shock and the tip vortex and then increases again closer to the pressure side. At high flow rates near design, radial distortion only slowed down the flow near the suction side and slightly increased the width of the low momentum zone. The depth of the velocity decrement was almost the same as in the clean case. When the flow rate decreased, the velocity also reduced to very low values around 10-15 *m/s* and the width nearly doubled. Applying radial distortion produced a different effect for each passage. For example, in passages 2 and 3 there were almost no changes in depth or width of the velocity profile. While in the passage 1 and 4 the velocity became negative up to -30 *m/s*. This helps to understand the earlier stall inception in the radial distortion case.

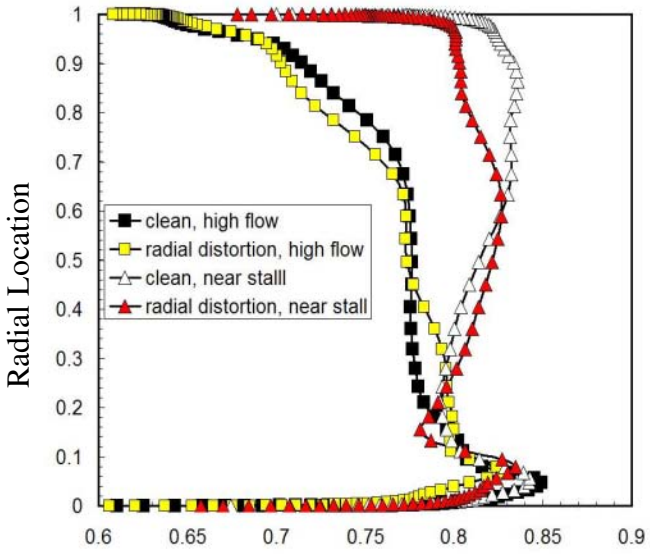

Figure 12. Radial total pressure distribution after the fan for 4 blades at 80% speed.

COMPARISON BETWEEN SPEED LINES

In the previous three sections the results of four blade simulations were presented for three speed lines from 100% to 80%. In all cases with clean inlet the work by the blade was done mainly by the upper part. Applying radial distortion had a different effect for 100% and 95% speeds than for 80%. At higher speeds the distortion produced noticeable flow separation near the hub extending up to 15% of the span. The total pressure ratio was reduced for all flow rates. At 80% speed no flow separation near the hub was observed and the total pressure slightly increased at lower flow rates.

There is evidence that the stronger shock at higher speeds has a stabilizing effect, because the communication between the passages from the upstream is not allowed due to the supersonic velocity at the inlet [21]. This leads to more similar flow pattern between the blades at higher speeds and to more

sudden transition to stall. Also the front shock leads to slower growth rate of the low momentum zone (which contributes to passage blockage). Radial distortion had only a small effect on the lowest value of the velocity at higher speeds, while at 80% it increased the depth and width of the velocity deficit.

CONCLUSIONS

Computational simulations were performed for an isolated transonic fan blade row to investigate the effects of radial distortion on performance and stall margin and to identify the main flow features. The inlet profiles were taken from experimental data simulating the effect of a supersonic inlet assembly and had both hub and tip total pressure deficits.

Four blade solutions that allowed flow distribution between passages predicted the stall margin more closely than single blade solutions. The difference at higher speeds where the shock system precluded inter-blade communication was smaller. Near choking conditions, the flow was steady, but as stall was approached and the mass flow rate decreased, the flow lost blade-to-blade symmetry and became unsteady, while still remaining stable. The results suggest that the presence of the shock prevents communication between the passages from the upstream producing a stabilizing effect on the flow so that the flow stays steady longer at higher rotational speeds and then suddenly undergoes large variations. At lower speeds (still transonic) oscillations grow more gradually before becoming violently unstable.

For all speed lines the stall margin was reduced when radial distortion was present. However, the rate of reduction was smallest for full speed. Distortion caused a significant reduction in the total pressure ratio near the hub at full and 95% speeds and also induced hub corner stall. The developed separation near the hub did not propagate toward the tip, but was convected downstream where it can potentially affect the compressor. The development of low momentum zones near the pressure side at the blade tip contributes to passage blockage and thus is important for stall inception. Further research is needed to identify the role of this blockage as compared to flow separation on the suction side. The effects of radial distortion on those zones were tested. At near-stall conditions, the effect of the distortion was small at full speed. At the 80% speed, the circumferential width and minimum value of the velocity inside increased unevenly between passages.

ACKNOWLEDGMENTS

The authors would like to acknowledge Rolls-Royce and Gulfstream for providing funds for this research and allowing publication of the results.

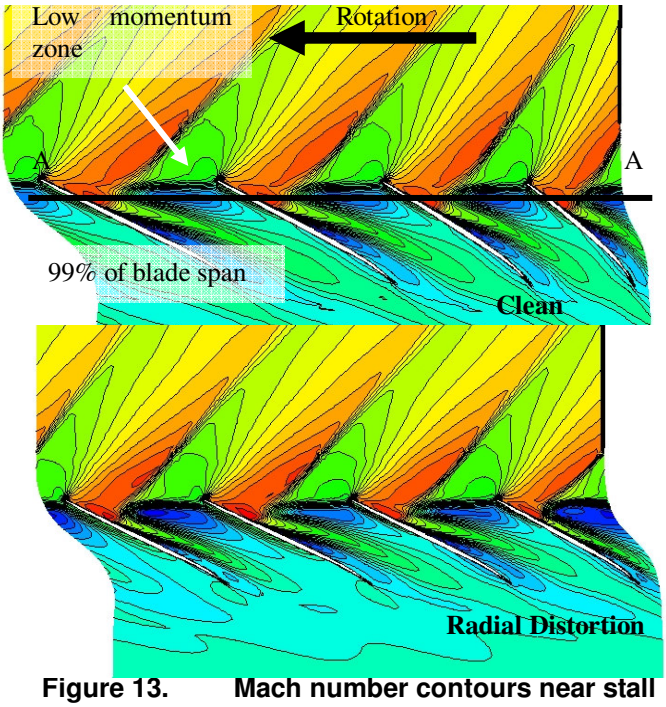

Figure 13. Mach number contours near stall at constant span near tip at 80% speed with clean (top) and distorted (bottom) inlets.

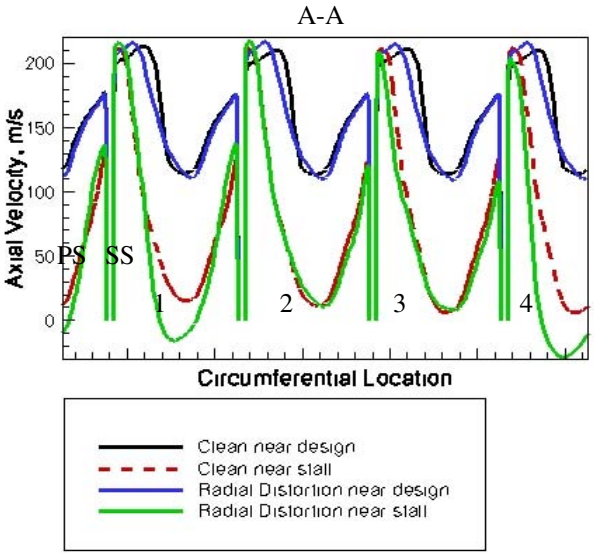

Figure 14. Axial velocity distribution along a 20% chord cut at 99% span; 80% speed.

REFERENCES

[1] Conners, T., R., Howe, D., C., "Supersonic Inlet Shaping for Dramatic Reductions in Drag and Sonic Boom Strength," AIAA paper 2006-0030, 2006.

[2] Conway, M., J., Lavely, A., W., Blaisdell. G., A., "A Computational Investigation of Flow Through an Axi-symmetric Supersonic Inlet," AIAA paper 2010-0941, 2010.

[3] Davis, M., Hale, A., Beale, D., "An Argument for Enhancement of the Distortion Inlet Distortion Ground Test Practice for Aircraft Gas Turbine Engines", *Journal of Turbomachinery*, Vol 124, 2002, pp 235-241.

[4] Bennington., M., Cameron., J., Morris., S., Legault., C., Barrows., S., Chen., J.-P., McNulty, G., S., Wadia., A., R.,"Investigation of Tip-Flow Based Stall Criteria Using Rotor Casing Visualization," Proceedings of ASME Turbo Expo 2008, Vol. 6, Pt A, 2008, pp. 641-651.

[5] Sandercock, D., M., Sanger, N., L., "Some Observations of the Effects of Radial Distortions on Performance of a Transonic Rotating Blade Row," 1979, NASA TN D-7824.

[6] Longley, J., P., Greitzer, E., M., "Inlet Distortion Effects on Aircraft Propulsion System Integration", AGARD-LS-183, 1992.

[7] Longley, J., P., Shin, H.,-W., Plumley, R., E., Silkowski, P., D., Day, I., J., Greitzer, E., M., Tan, C., S., and Wisler, D., C., "Effects of Rotating Inlet Distortion on Multistage Compressor Stability," *Journal of Turbomachinery*, Vol. 118, 1996, pp. 181-188.

[8] Hah, C., Rabe, D., C., Sullivan, T., C., Wadia, A., R., "Effects of Inlet Distortion on Flow Field in Transonic Compressor Rotor", *Journal of Turbomachinery*, Vol 120, 1998, pp 233-246.

[9] Charalambous, N., Ghisu, T., Lurisci, G., Pachidis, V., Pilidis, P., "Axial Compressor Response to Inlet Distortions by a CFD Analysis", GT2004-53846, pp. 1637-1650.

[10] Gorrell, S., E., Yao, J., Wadia, A., R.,"High Fidelity URANS Analysis of swirl Generation and Fan Response to Inlet Distortion," AIAA Paper 2008-4985.

[11] Choi, M., Oh, S., H., Ko., H., Y., Baek, J., H.,"Effects of the Inlet Boundary Layer thickness on Rotating Stall in an Axial Compressor," Proceedings of ASME Turbo Expo 2008, Vol. 6, Pt A, 2008, pp.497-507.

[12] Voytovych D., M., Merkle, C., L., Xia., G., "Analysis of Flows around Fan from Choke to Stall with Radial distortion," AIAA paper 2010-0745, 2010

[13] Sankaran, V. and Merkle, C.L. "Artificial Dissipation Control for Unsteady Computations," AIAA Paper 2003-3695, 2003.

[14] Li, D., Xia, G. and Merkle, C.L.," Analysis of Real Fluid Flows in Converging Diverging Nozzles," AIAA Paper 2003-4132, 2003.

[15] Chen, J., P., Ghosh, A., R., Sreenivas, K., Whitefield, D., L., "Comparison of Computations Using Navier-Stokes Equations in Rotating and Fixed Coordinates for Flow Through Turbomachinery", 35th AIAA Aerospace Sciences Meeting and Exhibit, AIAA Paper 1997-0878.

[16] Wilcox, D.C., *Turbulence Modeling for CFD*, 2nd ed.,DCW Industries, La Canada, CA, 1998.

[17] Vahdati, M, Sayma, AI, Freeman, C, and Imregun, M.,"On the Use of Atmospheric Boundary Conditions for Axial-Flow Compressor Stall Simulations," *Journal of Turbomachinery*, Vol. 127, 2005, pp. 349-351.

[18] Vo, H.-D., Tan, C., S., Greitzer, E., M., "Criteria for Spike Initiated Rotating Stall," *Journal of Turbomachinery*, Vol. 130, 2008, p. 011023.

[19] Niazi, S., "Numerical simulation of rotating stall and surge alleviation in axial compressor", PhD Dissertation, Georgia Institute of Technology, Dept of Aerospace Engineering, Atlanta, USA, 2000.

[20] Davis, R., Yao, J.,"Predictions of Compressor Stage Performance from Choke Through Stall," *Journal of Propulsion and Power,* Vol. 22, No 3, 2006, pp. 550-557.

[21] He, L., Ismael, J., O., "Computations of Bladerow Stall Inception in Transonic Flows", *The Aeronautical Journal,* Vol. 103, Issue 1025, pp 317-324.

[22] Gu, C., Feng., F., Li X., Chen., M.,"Application of Detached Eddy Simulation to a Subsonic Compressor Rotor," Proceedings of ASME Turbo Expo 2008, Vol. 6, Pt A, 2008, pp.131-138.

[23] Hah, C., Rabe, D., Wadia, A., R., "Role of Tip-Leakage Vorticies and Passage Shock in Stall Inception in a Swept Transonic Compressor Rotor", Proceedings of ASME Turbo Expo 2004, Vol.5, Pt. A, pp. 545-555

[24] Chima, R., "Calculation of Tip Effects in a Transonic Compressor Rotor", *Journal of Turbomachinery*, Vol 120, 1998, pp 131-140.

[25] Adamczyk, J., J., Celestina, M., L., Greitzer, E., M., "The Role of Tip Clearance in High-Speed Fan Stall", *Journal of Turbomachinery*, Vol. 115, 1993, pp. 28-38.